Observer-based Finite-time Convergence Guidance Law with Autopilot Dynamic Lag Compensation and Attack Angle Constraint

Shuai Xu, Min Gao, Dan Fang, Yi Wang, Baochen Li

Abstract—**In this paper, a guidance problem with attack angle when missile attacks ground target is investigated. On the basis of high-order guidance model including the second-order autopilot dynamic lag, a nonsingular terminal sliding mode guidance law with attack angle constraint is proposed. In the design, nonsingular terminal sliding mode certifies that the line-of-sight (LOS) angle rate could converge to zero and the attack angle could reach the desired value within a finite time. Besides, the derivatives of virtual control variables and disturbance terms are estimated together by the extended state observer (ESO) with improved nonlinear feedback function, and the estimates are applied to compensate the control quantities, which could help the law resist the disturbances. Dynamic surface control plays a major role in completing the control law for a high-order system. According to the Lyapunov stability theory, all states in the closed loop system are proved to ultimately converge into a little neighborhood of the origin. Simulation results demonstrate that the proposed guidance law can obtain more accurate terminal LOS angle and smaller miss-distance.**

Index Terms—**guidance law, dynamic surface control, extended state observer, autopilot dynamic lag compensation, attack angle constraint, finite-time convergence**

I. Introduction

A certain type of homing anti-tank missile is configured for top attack to destroy targets. In order to raise the lethality of warhead, small miss distance and desired attack angle are expected. Under different application backgrounds, many scholars have studied a variety of guidance laws with angle constraints on the basis of different theories, such as optimal guidance law[1-2], biased proportional guidance law[3-4], differential game guidance law[5], and so on. However, the guidance laws above are limited by assumptions, their demands on precision of target motion model and accuracy of status information are higher, and disturbance rejection capabilities are not strong. The sliding mode variable structure control is not strictly dependent on precise target motion model, which can compensate system uncertainties by the discontinuous switching term. It has strong robustness and stability to external disturbances and system parameter uncertainties, and is extensively used in the guidance law design.

The guidance law with attack angle constraint can be easily obtained via introducing attack angle constraint in sliding mode surface design. Linear sliding hyperplane[6-7] is normally chosen in the traditional sliding mode design. The tracking errors of system states on traditional sliding mode surface gradually converges to zero, and the convergent speed is regulated via the parameter matrix of sliding mode surface. Obviously, this design method cannot meet the requirement of finite-time convergence. To enforce system states converge in finite time, nonlinear term was introduced to construct terminal sliding mode surface[8-9], which can achieve the finite-time convergence of tracking error on the sliding mode surface. While, the derivative of terminal sliding mode surface has a negative exponent term that may cause singularity problem due to improper parameter selection or system state value. Hence, in practical applications, non-singular terminal sliding mode surface is more often used[10-12].

The autopilot dynamic is an important factor influencing the guidance accuracy. The guidance law considering autopilot dynamics can achieve seamless integration between the guidance law and the control law, which is helpful for improving the performance of overall system. The control instructions generated by the guidance law are tracked by the autopilot via adjusting the actuator, such as steering gears. According to the characteristics of aerodynamic control surfaces, the process from deflecting rudder surface to building a new projectile posture is influenced by the autopilot dynamics and the hardware of missile, which causes the delay from guidance instruction to actual acceleration. For the light homing anti-tank missile, due to the limitations of seeker performance, missile structure size, engine thrust and other factors, its range is short, and the terminal guidance time is finite. In order to hit the target accurately at a desired attack angle, a high-precision guidance law is required to drive the LOS angle rate to zero in finite time. However, the delay mentioned above will lead to a decrease in guidance accuracy. Generally, in the design process of sliding mode guidance law, the missile autopilot dynamics is considered as an ideal link without delay. In fact,

Manuscript received January 31th, 2019; revised May, 18th, 2019.

Shuai Xu is with the Army Engineering University, No.97 Heping West Road, Shijiazhuang, Hebei, 050003, China (corresponding author to provide e-mail: xushuai1239@163.com).

Min Gao is with the Army Engineering University, No.97 Heping West Road, Shijiazhuang, Hebei, 050003, China (e-mail: gaomin1103@yeah.net).

Dan Fang is with the Army Engineering University, No.97 Heping West Road, Shijiazhuang, Hebei, 050003, China (e-mail: aq_fd@126.com).

Yi Wang is with the Army Engineering University, No.97 Heping West Road, Shijiazhuang, Hebei, 050003, China (e-mail: wangyi050926 @ 163.com).

Baochen Li is with the Army Engineering University, No.97 Heping West Road, Shijiazhuang, Hebei, 050003, China (e-mail: 944275029@qq.com).

(Advance online publication: 12 August 2019)

introducing autopilot dynamics in the design of guidance law can help to cope with the mentioned delay effect.

Considering the autopilot dynamics will add the order of guidance system state equations. The backstepping method is usually applied to design control law for the high-order system, but it can easily lead to a problem of "differentiation expansion" after multiple derivations of virtual variables. In order to solve the problem, the dynamic surface control method was proposed by Swaroop[13], which combined the advantages of integral backstepping and multi-sliding mode control. Considering the autopilot dynamic lag, Y. Zhang[14] designed a global non-linear integral sliding mode guidance law(SMGL) with attack angle constraint by the dynamic surface control. P. P. Qu[15] proposed a guidance law with autopilot dynamic lag compensation by dynamic surface control, which had a well adaptability for changes of target maneuvering. Nevertheless, the attack angle constraint was not considered when the law was designed. J. Yang[16] took the autopilot second-order dynamic lag into account, used integral sliding mode to design the dynamic surface, and estimated the target maneuvering disturbance through the observer. But each step of dynamic surface design was asymptotically convergent, and the closed-loop system also asymptotically converged to the bound of steady-state error. Considering the autopilot first-order dynamic lag, H. J. Wang [17] designed a sliding mode guidance law by estimating guidance information through the ESO with a filter. But sliding mode surface of the law was linear and the system stability was not proved. Besides, via estimating target maneuvering by the ESO, S. F. Xiong[18] presented a guidance law by nonsingular terminal sliding mode and dynamic surface control, while, the law only took the first-order autopilot dynamic lag into consideration.

Along the technology mentioned above, in this paper, in consideration of the autopilot second-order dynamic lag, dynamic surface control is applied to construct a guidance law with attack angle constraint. The first dynamic surface of the law is designed with nonsingular terminal sliding mode surface, which could drive the states to converge into a little neighborhood of the origin. In order to avoid the problem of "differentiation expansion", the improved ESO with better convergence speed is applied to estimate disturbance terms and virtual control quantities. Besides, fast power reaching law is used to obtain the finite-time convergence stability. A kind of optimal discrete tracking differentiator (ODTD) is applied to estimate the derivation of missile acceleration. Finally, the closed-loop system is proved to be globally finite-time stable and simulation results illustrate the effectiveness of the method.

II. PROBLEM DESCRIPTION

A. Stage Missile-Target Relative Motion Equations

The skid-to-turn missile has axially symmetrical shape roll stabilized, thus the three channels can be decomposed into vertical plane motion and lateral plane motion. In flights at little angles of attack and side slip angles, the design method of vertical plane motion is similar to the lateral plane motion, therefore, this paper takes missile-target motion process in vertical plane as an example to analyze, which is shown in Fig.1.

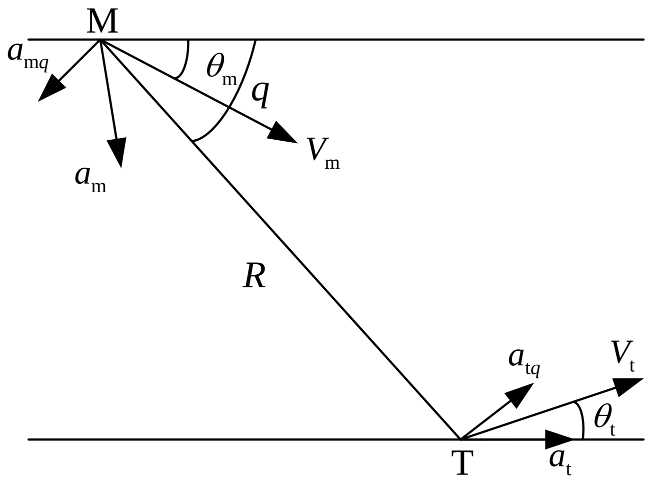

Fig.1. Missile-target relative motion in vertical plane

In Fig.1, the kinematic engagement equations are

$$\dot{R} = V_t \cos(q-\theta_t) - V_m \cos(q-\theta_m) \tag{1}$$

$$R\dot{q} = -V_t \sin(q-\theta_t) + V_m \sin(q-\theta_m) \tag{2}$$

M is the center of mass in missile and T is the target. The missile-target relative distance is denoted as R, and $\dot{R}$ is missile-target relative distance change rate. V_t and V_m represent the speeds of target and missile respectively. The LOS angle is represented as q, and its derivative is LOS angle rate $\dot{q}$. The flight-path angles of target and missile are written by θ_t and θ_m respectively.

Note that $V_R = \dot{R}$ and $V_q = R\dot{q}$, get the first order derivatives of V_R and V_q with respect to time as follow

$$\dot{V}_R = V_q^2 \big/ R + a_{tR} - a_{mR} \tag{3}$$

$$\dot{V}_q = -V_R V_q \big/ R + a_{tq} - a_{mq} \tag{4}$$

where a_{tR} and a_{mR} respectively are components of the target acceleration and missile acceleration in LOS direction, a_{tq} and a_{mq} are respectively used to represent the components of missile acceleration and target acceleration in normal direction of LOS.

The relative two-degree dynamics between the control input a_{mq} and the LOS angle q is given by

$$\ddot{q} = -\frac{2\dot{R}}{R}\dot{q} - \frac{1}{R}a_{mq} + \frac{1}{R}a_{tq} \tag{5}$$

In the terminal guidance process, the relative velocity $\dot{R} < 0$ is essential to satisfy the condition for missile-target approach. In the mean while, considering that the target has a certain size, the following inequalities are established[19]

$$\dot{R} < 0,\ R_{\min} < R < R_{\max} \tag{6}$$

where $R_{\max}$ is the maximum missile-target distance, $R_{\min}$ is the minimum missile-target distance formed by the target size.

The axial velocity is not controllable in the terminal guidance section, so the key of the guidance law design is to control the LOS angle rate $\dot{q}$ by a_{mq}, drive it approach a small neighborhood near zero[15].

B. Autopilot Model

The acceleration instruction generated by the guidance loop needs to be tracked by the autopilot. In order to avoid the impact of high-frequency un-modeled dynamics, the bandwidth of the autopilot is generally not high, so its dynamics may cause a certain dynamic lag for the execution of acceleration instruction and affect the guidance performance. Hence, the autopilot dynamics should be incorporated into the guidance law. Simplify the missile autopilot dynamics as a second-order link given by

$$\frac{a_{mq}}{u} = \frac{\omega_n^2}{s^2 + 2\xi\omega_n s + \omega_n^2} \tag{7}$$

where ξ and ω_n respectively are the relative damping coefficient and natural frequency of the missile autopilot, u is the normal acceleration instruction for the missile autopilot. Formula (7) can be expressed as a differential equation given by

$$\ddot{a}_{mq} = -2\xi\omega_n\dot{a}_{mq} - \omega_n^2 a_{mq} + \omega_n^2 u \tag{8}$$

C. Description of Terminal Attack Angle

Generally, the attack angle is defined as the angle between the velocity vectors of missile and target at the time of interception. Ignoring the smaller incident angle, attack angle also can be regarded as the included angle between missile attitude angle and target attitude angle[20]. Denote the guidance end time as t_f, the expected attack angle as θ_d, and the expected LOS angle as q_d. In order to improve the damage effect, attack angle constraint is the key to design the guidance law.

$$\lim_{t\to t_f} R(t)\dot{q}(t) = 0 \tag{9}$$

$$\theta_m(t_f) - \theta_t(t_f) = \theta_d \tag{10}$$

$$|\theta_m(t_f) - q_d| < \pi/2 \tag{11}$$

The inequality in (11) ensures that the missile can capture the target, in other words, the target is within the seeker's field of view during guidance process. It can be obtained from (2) and (9) that

$$V_m\sin(q_d - \theta_m) - V_t\sin(q_d - \theta_t) = 0 \tag{12}$$

Substituting (10) into (12) yields

$$V_m\sin(q_d - \theta_t(t_f) - \theta_d) - V_t\sin(q_d - \theta_t(t_f)) = 0 \tag{13}$$

By using (13) and applying trigonometric algebra, following equation can be written

$$q_d = \theta_t(t_f) - \tan^{-1}\left(\frac{\sin\theta_d}{\cos\theta_d - V_t/V_m}\right) \tag{14}$$

where $V_t/V_m < 1$. Formula (14) shows that for the given $\theta_t(t_f)$ and θ_d, there is an unique desired LOS angle q_d corresponding to them, so the attack angle constraint problem can be converted to a LOS angle tracking problem. Accordingly, The goal of guidance law design translates into driving $\dot{q} \to 0$ and $q \to q_d$.

D. Establishment of Guidance Equations

Define the state variables $x_1 = q - q_d$, $x_2 = \dot{q}$, $x_3 = a_{mq}$ and $x_4 = \dot{a}_{mq}$. Considering that the target acceleration is difficult to measure by the on-board device, its normal component on the LOS, denoted by a_{tq}, is regarded as an external disturbance d_1. At the same time, taking the uncertainty d_n caused by the autopilot model simplification error and aerodynamic parameter change into consideration[21], the guidance equations taking the second-order autopilot dynamics into account are given by

$$\begin{cases} \dot{x}_1 = x_2 \\ \dot{x}_2 = -\dfrac{2\dot{R}}{R}x_2 - \dfrac{1}{R}x_3 + \dfrac{1}{R}d_1 \\ \dot{x}_3 = x_4 \\ \dot{x}_4 = -\omega_n^2 x_3 - 2\xi\omega_n x_4 + \omega_n^2 u + d_n \end{cases} \tag{15}$$

There are physical limitations of energy and response speed in the target motion process[22], so it is assumed that the disturbances d_1 and d_n are differentiable and have upper bounds.

To achieve the attack angle constraint and hit the target, we need to design a control law to drive $x_1 \to 0$ and $x_2 \to 0$ in finite time.

III. Preliminary Concepts

Before the guidance law design, the finite-time stability criteria and some lemmas are introduced to provide a theoretical basis for the subsequent proof.

Lemma 1[23]: Consider the following nonlinear system

$$\dot{x} = f(x,t),\ f(0,t) = 0,\ x \in \mathbf{R}^n \tag{16}$$

where f: $\mathrm{U}_0 \times \mathbf{R} \to \mathbf{R}^n$ is continuous on $\mathrm{U}_0 \times \mathbf{R}$, and $\mathbf{U}_0$ is an open neighborhood of the origin $x = 0$. Suppose there is a $\mathbf{C}^1$ smooth and positive definite function $V(x,t)$ defined at $\mathbf{U} \subset \mathbf{R}^n$, which is the neighborhood of the origin, and exist real numbers $\alpha > 0$ and $0 < \lambda < 1$, making $V(x,t)$ be positive definite on $\mathbf{U}$ and $\dot{V}(x,t) + \alpha V^\lambda(x,t)$ be negative semi-definite on $\mathbf{U}$, then the system origin is finite-time stable. If $\mathbf{U} \subset \mathbf{R}^n$ and $V(x,t)$ is radially unbounded, then the system origin is globally finite-time stable. The convergence time, denoted by t_r, depends on the initial value x_0, the following inequality holds

$$t_r \le \frac{V(x_0,0)^{1-\lambda}}{\alpha(1-\lambda)} \tag{17}$$

where x_0 is any point in the open neighborhood of the origin.

Lemma 2[24]: For $\forall\alpha_1 > 0$, $\alpha_2 > 0$, $\eta \in (0,1)$, the smooth and positive definite Lyapunov function $V(x)$ that defines on $\mathbf{U} \subset \mathbf{R}^n$ satisfies

$$\dot{V}(x) + \alpha_1 V(x) + \alpha_2 V^\eta(x) \le 0 \tag{18}$$

then the system state x can converge to the origin in the finite time t_r, and

$$t_r \le \frac{1}{\alpha_1(1-\eta)} \ln[1+\frac{\alpha_1}{\alpha_2} V^{1-\eta}(x_0)] \tag{19}$$

where $V(x_0)$ is the initial value of $V(x)$.

Lemma 3[25]: For $\forall$ $x_i \in \mathbf{R}$ ($i = 1,2,\ldots,n$), and $\forall$ $0 < p \le 1$, the following inequality holds

$$\left(|x_1| + |x_2| + \cdots + |x_n|\right)^p \le |x_1|^p + |x_2|^p + \cdots + |x_n|^p \tag{20}$$

IV. Guidance Law Design

Considering the linear time-varying system in (15), this paper adopts dynamic surface control and reaching law method to design a finite-time convergence guidance law with terminal attack angle constraint. The disturbance term and derivative of virtual control of each subsystem are combined to be a total disturbance term, which can be estimated by the improved ESO. Through the method above, the first-order filter common in dynamic surface control is no longer needed to obtain the differential of virtual control.

A. The Improved ESO

ESO is first proposed by J. Q. Han[26-28]. It extends the uncertainty part of the system to be a new first-order state, and feedback errors via specific non-smooth and nonlinear function[29]. By selecting suitable parameters of ESO, the system states and disturbance terms will be estimated. It is a kind of generic and practical nonlinear disturbance observer, which does not rely on the concrete mathematical model. The stability of ESO has been proved by B.Z. Guo[30].

The second-order system to be observed is given as

$$\begin{cases} \dot{y}_1 = f(y_1) + y_2 \\ \dot{y}_2 = w \end{cases} \tag{21}$$

where $f(y_1)$ is the modeled dynamic part of the system, y_2 is the total of unmodeled dynamics and external disturbance, w is the derivative of disturbance. Based on (21), the ESO is designed as follow

$$\begin{cases} e = z_1 - y_1 \\ \dot{z}_1 = -\beta_{01} e + f(y_1) + z_2 \\ \dot{z}_2 = -\beta_{02}\, fal(e,\alpha,\delta_1,\gamma,\delta_2) \end{cases} \tag{22}$$

where, y_1 is the awaiting observation signal, z_1 is the estimation of y_1, z_2 is the estimation of y_2, β_{01} and β_{02} are the adjustable gain, $fal(e,\alpha,\delta_1,\gamma,\delta_2)$ is the non-smooth and nonlinear feedback function. Selecting the suitable parameters (i.e.: β_{01}, β_{02}, α, γ, δ_1, δ_2), it is easy to estimate the system state y_1 and disturbance y_2 via tracking the system state y_1. $fal(\bullet)$ function is defined as

$$fal(e,\alpha,\delta_1,\gamma,\delta_2) = \begin{cases} e/\delta_1^{1-\alpha} & |e| \le \delta_1 \\ |e|^\alpha \operatorname{sgn}(e) & \delta_1 < |e| < \delta_2 \\ \delta_2^{\alpha-\gamma} |e|^\gamma \operatorname{sgn}(e) & |e| \ge \delta_2 \end{cases} \tag{23}$$

where, $0 < \alpha < 1$, $\gamma \ge 1$, and $\delta_2 > \delta_1 > 0$ are the error threshold. The curve of $fal(\bullet)$ is shown in Fig. 2.

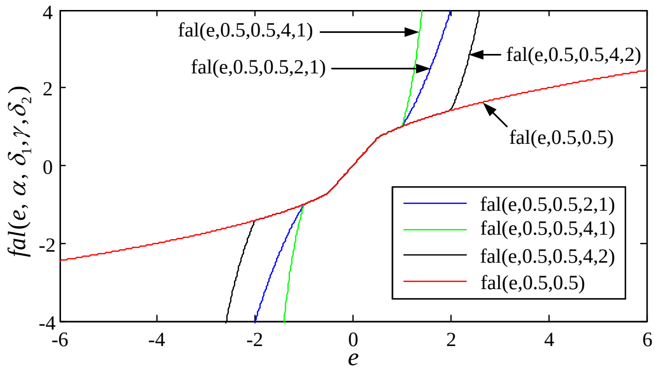

Fig.2. Curves of the $fal(\bullet)$ functions

As shown in Fig.2, when the tracking error keeps away from the balance point (i.e. $|e| \ge \delta_2$), $\delta_2^{\alpha-\gamma} |e|^\gamma \operatorname{sgn}(e)$ can accelerate the approach process to balance point, which effectively avoids the condition that the control quantity cannot increase quickly to reduce tracking error when the error is large. Taking the property of control quantity, error range and gain magnitude into consideration, δ_1 and δ_2 can be adjusted to meet different demands.

B. Guidance Law Design by Dynamic Surface Control

(1) Design the virtual control quantity $\bar{x}_3$ of x_3

The first subsystem in (24) is given as

$$\begin{cases} \dot{x}_1 = x_2 \\ \dot{x}_2 = -\frac{2\dot{R}}{R} x_2 - \frac{1}{R} x_3 + \frac{1}{R} d_1 \end{cases} \tag{24}$$

At the end of flight, R rapidly decreases, which leads to the increasing of d_1/R. The condition above requires that the ESO should deal with the variables varying in a large range. To reduce the design difficulty of ESO, (25) can be derived from (4) as follow

$$\dot{V}_q = -\dot{R} x_2 - x_3 + d_1 \tag{25}$$

Adopt the ESO to observe V_q, and then estimate d_1. d_1 is expanded into a new state, then (25) is extended to be a second-order system as

$$\begin{cases} \dot{V}_q = -\dot{R} x_2 - x_3 + d_1 \\ \dot{d}_1 = w_1(t) \end{cases} \tag{26}$$

where, $w_1(t)$ is the derivatives of d_1, $|w_1(t)| \le L_1$, and $L_1 > 0$ are the upper bound of $w_1(t)$. Based on (26), the second-order ESO is designed as (27). d_1 is restructured by z_{12} in a limited time.

$$\begin{cases} e_{11} = z_{11} - V_q \\ \dot{z}_{11} = -\beta_{11} e_{11} - \dot{R} x_2 - x_3 + z_{12} \\ \dot{z}_{12} = -\beta_{12}\, fal(e_{11},\alpha_1,\delta_{11},\gamma_1,\delta_{12}) \end{cases} \tag{27}$$

In order to satisfy the requirement that attack angle constraint and LOS angle rate simultaneously converge to zero in finite time, the first dynamic surface s_1 is defined as a non-singular terminal sliding surface in the form below

$$s_1 = x_1 + x_2^{m/n}/\beta_1 \tag{28}$$

where $\beta_1 > 0$ is a constant, m and n are positive odd numbers, which satisfy $1 < m/n < 2$.

The derivative of s_1 is given as

$$\begin{aligned}\dot{s}_1 &= x_2 + \frac{m}{\beta_1 n} x_2^{m/n-1}\dot{x}_2 \\ &= x_2 + \frac{m}{\beta_1 n} x_2^{m/n-1}(-\frac{2\dot{R}}{R}x_2 - \frac{1}{R}x_3 + \frac{1}{R}d_1)\end{aligned} \tag{29}$$

The adaptive fast power reaching law is designed as

$$\dot{s}_1 = -k_1\frac{|\dot{R}|}{R}s_1 - \frac{\varepsilon_1}{R}|s_1|^{\eta}\operatorname{sgn}(s_1) \tag{30}$$

where $k_1 > 0$, $\varepsilon_1 > 0$ and $0 < \eta < 1$. The performance of reaching law is mainly affected by k_1 and ε_1. Increasing k_1 and ε_1 can improve the approaching speed. However, the larger k_1 will enlarge control instruction and required overload; the larger ε_1 can magnify the system chattering. Therefore, a few corrections are needed to get suitable parameters.

By the constructed disturbance term z_{12}, in order to make the system states reach the sliding mode surface s_1 and satisfy $s_1 \to 0$ in a finite time, which make $x_1 \to 0$ and $x_2 \to 0$, $\bar{x}_3$ is designed as

$$\begin{aligned}\bar{x}_3 = &-2\dot{R}x_2 + R\beta_1\frac{n}{m}x_2^{2-m/n} + k_1|\dot{R}|s_1 + \varepsilon_1|s_1|^{\eta}\operatorname{sgn}(s_1) \\ &+ z_{12}\end{aligned} \tag{31}$$

(2) Design the virtual control quantity $\bar{x}_4$ of x_4

The error surface is defined as $s_2 = x_3 - \bar{x}_3$, with the derivative of s_2, there is $\dot{s}_2 = x_4 - \dot{\bar{x}}_3$. $-\dot{\bar{x}}_3$ is regarded as disturbance (i.e. d_2), and d_2 is extended to be a new state, which is given as

$$\begin{cases}\dot{s}_2 = x_4 + d_2 \\ \dot{d}_2 = w_2(t)\end{cases} \tag{32}$$

where $w_2(t)$ is the derivative of d_2. Because $\dot{\bar{x}}_3$ is a bounded physical quantity, it satisfies $|w_2(t)| \le L_2$, where $L_2 > 0$ is the upper bound of $w_2(t)$.

Through the second order ESO in (33), d_2 is reconstructed by z_{22} in finite time.

$$\begin{cases}e_{21} = z_{21} - s_2 \\ \dot{z}_{21} = -\beta_{21}e_{21} + x_4 + z_{22} \\ \dot{z}_{22} = -\beta_{22}\,fal(e_{21}, \alpha_2, \delta_{21}, \gamma_2, \delta_{22})\end{cases} \tag{33}$$

To make $s_2 \to 0$, and then $x_3 \to \bar{x}_3$, with z_{22} and $\dot{s}_2 = -k_2 s_2 - \varepsilon_2|s_2|^{\eta}\operatorname{sgn}(s_2)$ ($k_2 > 0$, $\varepsilon_2 > 0$, $0 < \eta < 1$), $\bar{x}_4$ is designed as

$$\bar{x}_4 = -k_2 s_2 - \varepsilon_2|s_2|^{\eta}\operatorname{sgn}(s_2) - z_{22} \tag{34}$$

(3) Design actual control quantity u

The error surface is defined as $s_3 = x_4 - \bar{x}_4$, with the derivative of s_3, there is $\dot{s}_3 = -2\xi\omega_n x_4 - \omega_n^2 x_3 + \omega_n^2 u + d_n - \dot{\bar{x}}_4$. $d_n - \dot{\bar{x}}_4$ is regarded as disturbance (i.e. d_3), and d_3 is extended to be a new state, which is given as

$$\begin{cases}\dot{s}_3 = -2\xi\omega_n x_4 - \omega_n^2 x_3 + \omega_n^2 u + d_3 \\ \dot{d}_3 = w_3(t)\end{cases} \tag{35}$$

where, $w_3(t)$ is the derivative of d_3. Because $d_n - \dot{\bar{x}}_4$ is the bounded physical quantity, it satisfies $|w_3(t)| \le L_3$, where $L_3 > 0$ is the upper bound of $w_3(t)$.

Via the second order ESO in (36), in a finite time, d_3 is reconstructed by z_{32}.

$$\begin{cases}e_{31} = z_{31} - s_3 \\ \dot{z}_{31} = -\beta_{31}e_{31} - 2\xi\omega_n x_4 - \omega_n^2 x_3 + \omega_n^2 u + z_{32} \\ \dot{z}_{32} = -\beta_{32}\,fal(e_{31}, \alpha_3, \delta_{31}, \gamma_3, \delta_{32})\end{cases} \tag{36}$$

To make $s_3 \to 0$, and then $x_4 \to \bar{x}_4$, with z_{31} and $\dot{s}_3 = -k_3 s_3 - \varepsilon_3|s_3|^{\eta}\operatorname{sgn}(s_3)$ ($k_3 > 0$, $\varepsilon_3 > 0$, $0 < \eta < 1$), u is designed as

$$u = \frac{1}{\omega_n^2}(\omega_n^2 x_3 + 2\xi\omega_n x_4 - k_3 s_3 - \varepsilon_3|s_3|^{\eta}\operatorname{sgn}(s_3) - z_{32}) \tag{37}$$

C. Stability Analysis of Closed-loop System

The closed-loop system can be expressed as

$$\begin{cases}\dot{s}_1 = \dfrac{\lambda_1(x_2)}{R}(-k_1|\dot{R}|s_1 - \varepsilon_1|s_1|^{\eta}\operatorname{sgn}(s_1) + \Delta_1) \\ \dot{s}_2 = -k_2 s_2 - \varepsilon_2|s_2|^{\eta}\operatorname{sgn}(s_2) + \Delta_2 \\ \dot{s}_3 = -k_3 s_3 - \varepsilon_3|s_3|^{\eta}\operatorname{sgn}(s_3) + \Delta_3\end{cases} \tag{38}$$

In (38), $\lambda_1(x_2) = m x_2^{m/n-1}/(\beta_1 n)$, and by the values of m and n, there is $\lambda_1(x_2) \ge 0$, besides, the $\Delta_1 = d_1 - z_{12}$, $\Delta_2 = d_2 - z_{22}$ and $\Delta_3 = d_3 - z_{32}$ are estimation errors of disturbance observers. The second-order ESO is convergent in finite time[31] and its estimation error is small enough by selecting suitable parameters[32]. Note that the convergence of the observer is independent, which has no connection with the convergence of guidance system.

A positive definite and differentiable Lyapunov function for the closed-loop system is defined as

$$V = V_1 + V_2 + V_3 \tag{39}$$

where $V_1 = s_1^2/2$, $V_2 = s_2^2/2$ and $V_3 = s_3^2/2$.

Take the derivative of time with respect to V along the system in (38), there is

$$\begin{aligned}\dot{V} &= \dot{V}_1 + \dot{V}_2 + \dot{V}_3 = s_1\dot{s}_1 + s_2\dot{s}_2 + s_3\dot{s}_3 \\ &= \frac{\lambda_1(x_2)}{R}(-k_1|\dot{R}|s_1^2 - \varepsilon_1|s_1|^{\eta+1} + \Delta_1 s_1) \\ &\quad + (-k_2 s_2^2 - \varepsilon_2|s_2|^{\eta+1} + \Delta_2 s_2) \\ &\quad + (-k_3 s_3^2 - \varepsilon_3|s_3|^{\eta+1} + \Delta_3 s_3)\end{aligned} \tag{40}$$

Considering that $\dot{V}_1$, $\dot{V}_2$ and $\dot{V}_3$ have the same form, $\dot{V}_1$ is analyzed for example, and its conclusion is also applied to $\dot{V}_2$ and $\dot{V}_3$.

$$\begin{aligned}\dot{V}_1 &= \frac{\lambda_1(x_2)}{R}(-k_1|\dot{R}|s_1^2 - \varepsilon_1|s_1|^{\eta+1} + \Delta_1 s_1) \\ &\le \frac{\lambda_1(x_2)}{R_{\max}}(-k_1|\dot{R}|s_1^2 - \varepsilon_1|s_1|^{\eta+1} + |\Delta_1||s_1|)\end{aligned} \quad (41)$$

The analysis shows that when $s \neq 0$, formula (41) can be converted into the following two cases

$$\dot{V}_1 \le \frac{\lambda_1(x_2)}{R_{\max}}[-(k_1|\dot{R}| - |\Delta_1|/|s_1|)|s_1|^2 - \varepsilon_1|s_1|^{\eta+1}] \quad (42)$$

and

$$\dot{V}_1 \le \frac{\lambda_1(x_2)}{R_{\max}}[-k_1|\dot{R}||s_1|^2 - (\varepsilon_1 - |\Delta_1|/|s_1|^{\eta})|s_1|^{\eta+1}] \quad (43)$$

When $s_1 \neq 0$, due to $\lambda_1(x_2) \ge 0$, there is $\dot{V}_1 \le 0$ if k_1 and ε_1 are chosen appropriately. It can be proved that $x_2 = 0$ and $x_1 \neq 0$ are not a stable state and the state of $\dot{V}_1 = 0$ cannot be maintained, therefore, the system state can reach the sliding surface in a certain time.

For (42), when $|s_1| > |\Delta_1|/(k_1|\dot{R}|)$, there is

$$\begin{aligned}\dot{V}_1 &\le \frac{\lambda_1(x_2)}{R_{\max}}(-\bar{k}_1|s_1|^2 - \varepsilon_1|s_1|^{\eta+1}) \\ &\le \frac{\lambda_1(x_2)}{R_{\max}}(-2\bar{k}_1 V_1 - 2^{\frac{\eta+1}{2}}\varepsilon_1 V_1^{\frac{\eta+1}{2}})\end{aligned} \quad (44)$$

where $\bar{k}_1 = k_1|\dot{R}| - |\Delta_1|/|s_1| > 0$.

From lemma 2, the sliding surface s_1 converges in a finite time, and $\Omega_1 = \left\{ s_1 \,|\, |s_1| \le |\Delta_1|/(k_1|\dot{R}|) \right\}$ is the convergence domain. At the boundary of the convergence domain $|s_1| = |\Delta_1|/(k_1|\dot{R}|)$, $\dot{V}_1$ satisfies

$$\dot{V}_1 \le -\lambda_1(x_2)\varepsilon_1|\Delta_1|^{\eta+1}/(k_1|\dot{R}|R_{\max}) < 0 \quad (45)$$

According to LaSalle's invariant theory, Ω_1 is an invariant set of subsystem. Therefore, if $s_1(t_1) \in \Omega_1$ at time t_1, then for $\forall t > t_1$, there is $s_1(t) \in \Omega_1$.

For $|s_1| > \left(|\Delta_1|/\varepsilon_1\right)^{1/\eta}$, $\dot{V}_1$ in (43) is described by

$$\begin{aligned}\dot{V}_1 &\le \frac{\lambda_1(x_2)}{R_{\max}}(-k_1|\dot{R}||s_1|^2 - \bar{\varepsilon}_1|s_1|^{\eta+1}) \\ &\le \frac{\lambda_1(x_2)}{R_{\max}}(-2k_1|\dot{R}|V_1 - 2^{\frac{\eta+1}{2}}\bar{\varepsilon}_1 V_1^{\frac{\eta+1}{2}})\end{aligned} \quad (46)$$

where $\bar{\varepsilon}_1 = \varepsilon_1 - |\Delta_1|/|s_1|^{\eta}$. Similarly, it can be proved that s_1 can enter the convergence domain $\Omega_2 = \left\{ s_1 \,|\, |s_1| \le \left(|\Delta_1|/\varepsilon_1\right)^{1/\eta} \right\}$ in a finite time.

In summary, within a finite time, s_1 can be stable in a small neighborhood Φ_1 containing the origin.

$$\Phi_1 = \left\{ s_1 \middle| |s_1| \le \min\left(|\Delta_1|/\left(k_1|\dot{R}|\right),\ \left(|\Delta_1|/\varepsilon_1\right)^{1/\eta} \right) \right\} \quad (47)$$

Outside the Φ_1, there is

$$\dot{V}_1 \le \frac{\lambda_1(x_2)}{R_{\max}}(-2\min(\bar{k}_1, k_1|\dot{R}|)V_1 - 2^{\frac{\eta+1}{2}}\bar{\varepsilon}_1 V_1^{\frac{\eta+1}{2}}) \quad (48)$$

Similarly, the analysis of $\dot{V}_2$ 、 $\dot{V}_3$ shows that s_2 and s_3 can be stable within neighborhood Φ_2 and Φ_3 in finite time.

$$\Phi_2 = \left\{ s_2 \middle| |s_2| \le \min\left(|\Delta_2|/k_2,\ \left(|\Delta_2|/\varepsilon_2\right)^{1/\eta} \right) \right\} \quad (49)$$

$$\Phi_3 = \left\{ s_3 \middle| |s_3| \le \min\left(|\Delta_3|/k_3,\ \left(|\Delta_3|/\varepsilon_3\right)^{1/\eta} \right) \right\} \quad (50)$$

Outside the Φ_2 and Φ_3, $\dot{V}_2$ and $\dot{V}_3$ satisfy (51) and (52) respectively.

$$\dot{V}_2 \le -2\bar{k}_2 V_2 - 2^{\frac{\eta+1}{2}}\bar{\varepsilon}_2 V_2^{\frac{\eta+1}{2}} \quad (51)$$

$$\dot{V}_3 \le -2\bar{k}_3 V_3 - 2^{\frac{\eta+1}{2}}\bar{\varepsilon}_3 V_3^{\frac{\eta+1}{2}} \quad (52)$$

where $\bar{k}_2 > 0$, $\bar{\varepsilon}_2 > 0$, $\bar{k}_3 > 0$ and $\bar{\varepsilon}_3 > 0$. If the observation errors are small enough, by properly selecting the parameters k_1, ε_1, k_2, ε_2, k_3 and ε_3, each neighborhood domain can be sufficiently small to ensure that the system states are as close to zero as possible.

Introduce a new vector $\boldsymbol{s} = [s_1, s_2, s_3]^{\mathrm{T}}$ for the closed-loop system, when $\boldsymbol{s} \notin \Phi$ ($\Phi = \left\{ \boldsymbol{s} \middle| s_1 \in \Phi_1 \text{ and } s_2 \in \Phi_2 \text{ and } s_3 \in \Phi_3 \right\}$), in combination with Lemma 3, there is

$$\begin{aligned}\dot{V} &\le -2\frac{\lambda_1(x_2)\min(\bar{k}_1, k_1|\dot{R}|)}{R_{\max}}V_1 - 2\bar{k}_2 V_2 - 2\bar{k}_3 V_3 \\ &\quad - 2^{\frac{\eta+1}{2}}\frac{\lambda_1(x_2)}{R_{\max}}\bar{\varepsilon}_1 V_1^{\frac{\eta+1}{2}} - 2^{\frac{\eta+1}{2}}\bar{\varepsilon}_2 V_2^{\frac{\eta+1}{2}} - 2^{\frac{\eta+1}{2}}\bar{\varepsilon}_3 V_3^{\frac{\eta+1}{2}} \\ &\le -2\min\left\{ \frac{\lambda_1(x_2)\min(\bar{k}_1, k_1|\dot{R}|)}{R_{\max}}, \bar{k}_2, \bar{k}_3 \right\} V \\ &\quad - 2^{\frac{\eta+1}{2}}\min\left\{ \frac{\lambda_1(x_2)}{R_{\max}}\bar{\varepsilon}_1, \bar{\varepsilon}_2, \bar{\varepsilon}_3 \right\} V^{\frac{\eta+1}{2}} \\ &\le -c_1 V - c_2 V^{\frac{\eta+1}{2}}\end{aligned} \quad (53)$$

where $c_1 = 2\min\left\{ \lambda_1(x_2)\min(\bar{k}_1, k_1|\dot{R}|)/R_{\max}, \bar{k}_2, \bar{k}_3 \right\}$, $c_2 = 2^{(\eta+1)/2}\min\left\{ \lambda_1(x_2)/R_{\max}, \bar{\varepsilon}_1, \bar{\varepsilon}_2, \bar{\varepsilon}_3 \right\}$.

In terms of Lemma 1 and Lemma 2, the closed-loop system is globally finite-time stable, and the system state $\boldsymbol{s}$ can converge into a small neighborhood near zero in finite time. According to the finite time convergence characteristic of nonsingular terminal sliding mode surface s_1, the system states x_1 and x_2 can also converge into a small neighborhood near zero in a finite time.

D. Acquisition of Missile Acceleration Derivative

In order to obtain the accurate derivative information of missile acceleration component, an optimal discrete-time tracking differentiator (ODTD) in [33] is used. The expressions of ODTD are

$$\begin{cases} x_1(k+1) = x_1(k) + hx_2(k) + 0.5uh^2 \\ x_2(k+1) = x_2(k) + hu \\ u = f_c(x_1(k) - v(k), x_2(k), r, h) \end{cases} \tag{54}$$

$$\begin{cases} y = 2x_1 + hx_2, \quad s = \mathrm{sgn}(y) \\ k_0 = \dfrac{1}{2}\left(\sqrt{1 + \dfrac{4|y|}{h^2 r}} - 1\right) \\ k = fix(k_0) + 1 \\ f_c(x_1, x_2, r, h) = -\mathrm{sat}\left(\dfrac{x_2}{h} + \dfrac{(k-1)rs}{2} + \dfrac{y}{2kh^2}, r\right) \end{cases} \tag{55}$$

where h is the integral step, r is a parameter adjusting the tracking speed, $\mathrm{sgn}(\bullet)$ is the symbol function, $fix(\bullet)$ is the integral function rounding towards zero, and $\mathrm{sat}(\bullet)$ is saturation function, which is expressed as

$$\mathrm{sat}(x,\delta) = \begin{cases} \delta\,\mathrm{sgn}(x) & |x| > \delta \\ x & |x| \le \delta \end{cases} \tag{56}$$

V. Simulation Verification

To verify the validity of guidance law designed in this paper, this section conducts mathematical simulation. In the simulation, the missile and target are both moving in the pitch plane, and the guidance period is 10ms. The initial values of various parameters used in simulation are chosen to be X_{m0} =0, Y_{m0} =200m, V_m =110m/s, θ_{m0} =5°, ξ =0.7, ω_n =8rad/s, X_{t0} =1200m, Y_{t0} =0, V_{t0} =2m/s, θ_{t0} =0°. According to design indicator, the desired attack angle q_d is selected to be -35°. The design parameters of guidance law are chosen as $m=5$, $n=3$, $\beta_1=0.09$, k_1 =3, ε_1 =0.5, k_2 =10, ε_2 =0.5, k_3 =10, ε_3 =0.5 and $\eta=0.5$. Parameters of the second-order ESO are set to be $\alpha_i=0.5$, $\gamma_i=1$, $\delta_{i1}=0.5$, $\delta_{i2}=1$, $\beta_{i1}=100$ and $\beta_{i2}=500$, where $i=1,2,3$. The parameters of tracking differentiator are set as $h=0.01$ and $r=1500$. A technique that has been used to reduce chattering is to adopt a continuous approximation of the discontinuous control. Following this technique, the discontinuous function $\mathrm{sgn}(s)$ is approximated by the high-gain continuous function as $\zeta(s) = s/(|s|+\delta)$, where δ is a small positive number and set to be 0.001.

In combination with the requirements of design indexes and the actual situation on the battlefield, the ground moving target cannot make complex motion form because of the battlefield environment limitation, so three kinds of typical situations suitable for ground targets are set up in simulation: (1) Stationary target; (2) The target is evenly accelerated from 0m/s to 15m/s with the acceleration of 4m/s^2, and then it moves at a constant speed; (3) The target is accelerated from 2m/s to 15m/s with a varying acceleration $a_{tx}=4|\sin(t)|$ m/s^2, and then it moves at a constant speed. Simulation results are given in Table I and shown in Fig.3-6. In Table I, t_f is the end time of guidance process.

TABLE I
$R(t_f)$ AND $q(t_f)$ UNDER THREE TARGET MOTION SITUATIONS

Motion Situation	$R(t_f)$ (m)	$q(t_f)$ (°)
Situation 1	0.0787	-34.98
Situation 2	0.2717	-34.97
Situation 3	0.1066	-34.94

As shown in Table I, the guidance law adapts well to different target motion situations. In situation 1, because the target is still, the miss distance is minimal. In situation 2, this distance is the largest because of the maximal acceleration of the target. But, the miss distances in three situations are all less than 0.3m. The terminal LOS angle is very close to the desired value of -35°, and the angle deviation is less than 0.1°.

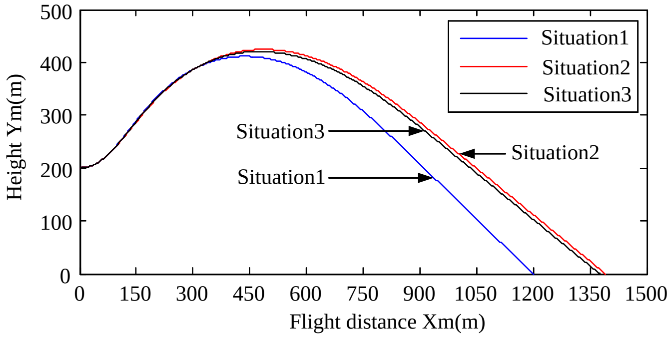

Fig.3. Curves of missile trajectories

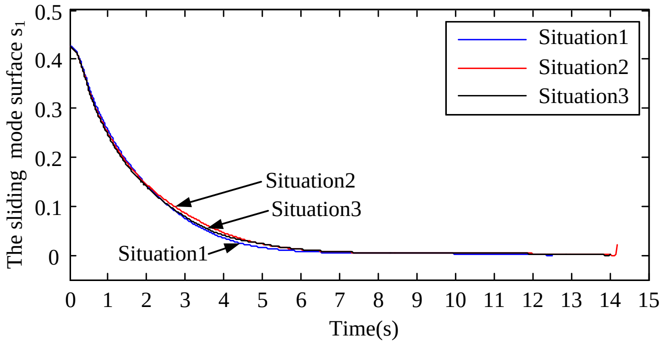

Fig.4. Curves of nonsingular terminal sliding mode surfaces

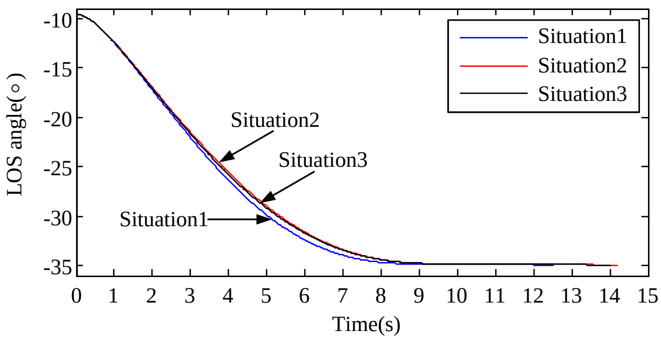

Fig.5. Curves of LOS angles

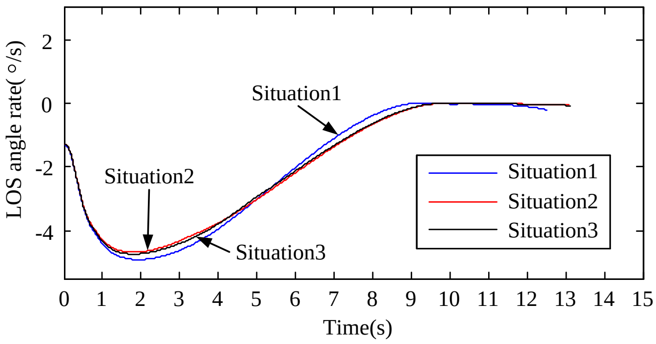

Fig.6. Curves of LOS angle rates

As can be seen in Fig.3, in order to obtain a larger terminal LOS angle, a higher trajectory occurs. The terminal trajectories are relatively straight after satisfying the LOS angle rate and LOS angle constraints, which is advantageous to the flight stability of missile and improvement of guidance precision.

From Fig.4 to Fig.6, it can be observed that, the nonsingular terminal sliding mode surface s_1 converges to near zero in a finite time, which makes the LOS angle rate also approach zero and the LOS angle reaches the desired value. As shown in Fig.4, s_1 in both laws converge to the interval (-0.01, 0.01) after the 7th second. It can be seen from Fig.5, the LOS angles converge into the interval (-35°, -34.8°) after the 10th second. The LOS angle rates converge to the interval (-0.05, 0.05) after the 9.5th second, as shown in Fig.6.

Taking the guidance process in situation 3 as an example, the improved ESO can quickly track V_q and the target maneuvering acceleration in normal direction of LOS can be effectively estimated in a short time. The estimation effects are shown in Fig.7-8.

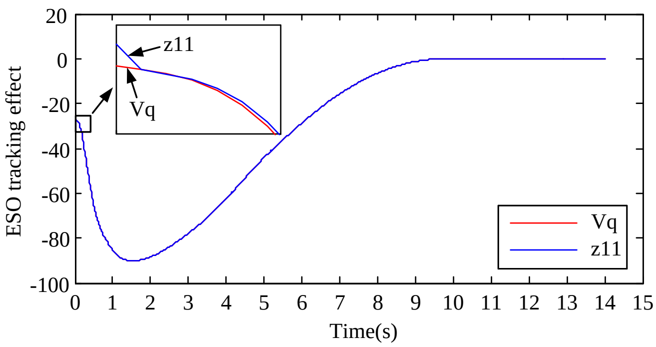

Fig.7. ESO tracking effect

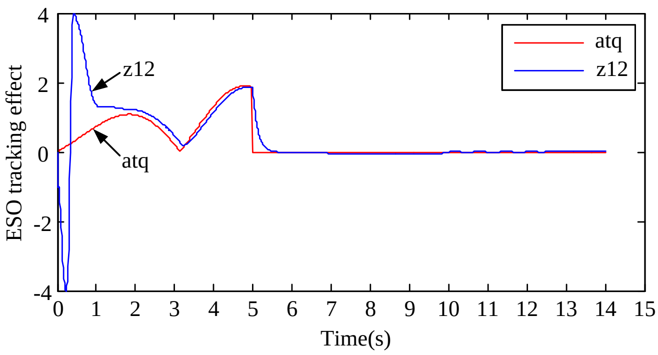

Fig.8. Acceleration component estimation of ESO

At the same time, in simulation process, the ODTD can effectively estimate x_4, as shown in Fig.9-10.

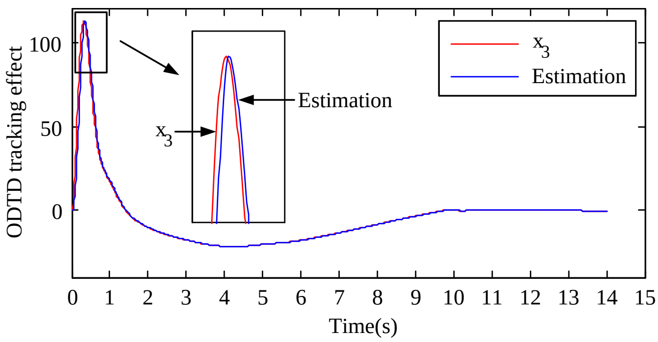

Fig.9. ODTD tracking effect

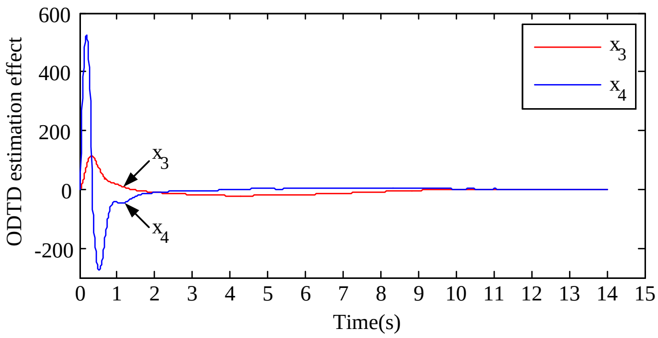

Fig.10. Estimation effect of x_4

Good tracking effect is a guarantee of effective estimation. As shown in Fig.9, ODTD can quickly track the dramatic changes in x_3. In Fig.10, x_4 increases rapidly when x_3 has a rapid rise. Then x_3 increases with a slower speed, at the same time, x_4 decreases quickly but it is still positive. When x_3 decreases quickly, x_4 changes from a positive value to a negative value and its absolute value increases rapidly. At last, after the change magnitude of x_3 decreases, x_4 also decreases accordingly. It can be seen from the above analysis that ODTD can effectively obtain variable differentiation and provide strong support for algorithm implementation.

In this subsection, in order to further verify the guidance performance, the attack effect of the missile with a shorter initial missile-target distance of 800m is investigated under three kinds of target motion situations, as shown in Table II and Fig.11-14.

TABLE II

$R(t_f)$ AND $q(t_f)$ UNDER THREE TARGET MOTION SITUATIONS

Motion Situation	$R(t_f)$ (m)	$q(t_f)$ (°)
Situation 1	-0.0768	-35.03
Situation 2	-0.3519	-35.03
Situation 3	-0.1001	-35.02

It can be seen from Table II that when the initial missile-target distance is shortened, the designed guidance law adapts well to different target motion situations, and the miss distance is less than 0.5m. At the same time, the terminal LOS angle is very close to the desired LOS angle of -35°, and the angle deviation is less than 0.1°.

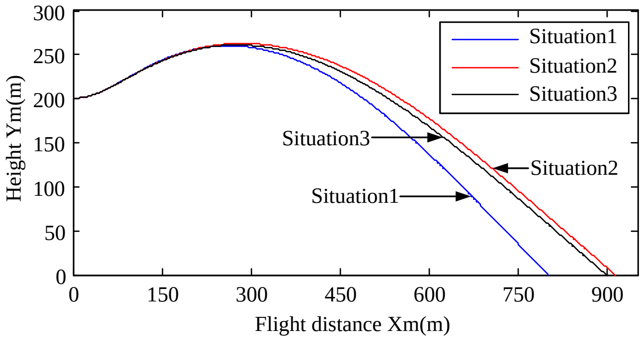

Fig.11. Curves of missile trajectories

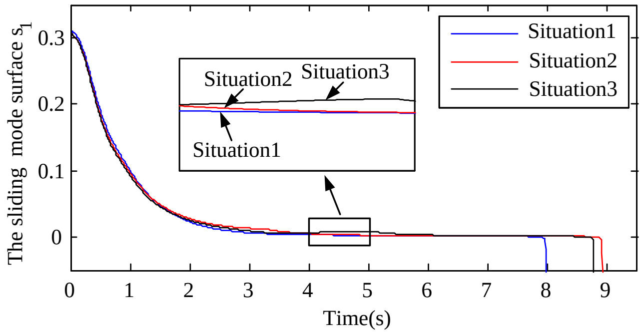

Fig.12. Curves of nonsingular terminal sliding mode surface s_1

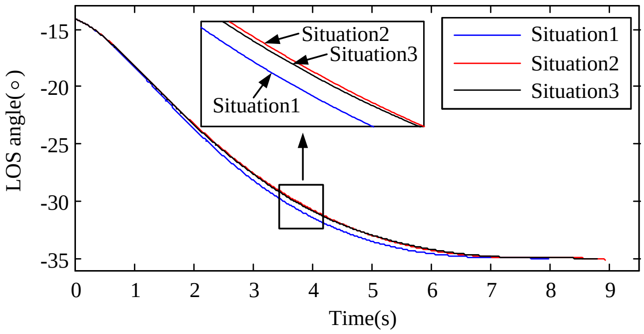

Fig.13. Curves of LOS angles

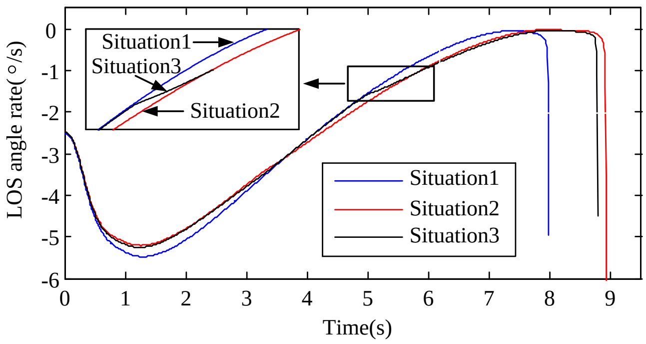

Fig.14. Curves of LOS angle rates

It can be seen from Fig.11 to Fig.14 that the nonsingular terminal sliding mode surface s_1 converges to near zero in a finite time, so that the LOS angle rate approaches zero and the LOS angle converges to the desired angle before hitting the target.

In this subsection, a comparison of the guidance law proposed in this paper is done with a nonsingular terminal sliding mode guidance law in [12], which is shown as

$$s=(q-q_{\mathrm{d}})+\beta\dot{q}^{\alpha} \tag{57}$$

$$u=\frac{1}{\cos(q-\theta_{\mathrm{m}})}\left(\frac{R}{\alpha\beta}\dot{q}^{2-\alpha}+2\dot{R}\dot{q}\right)+\frac{M}{\mathrm{sgn}(\cos(q-\theta_{\mathrm{m}}))}\mathrm{sgmf}(s) \tag{58}$$

where $\alpha=5/3$, $\beta=10$ and $M=80$. The function $\mathrm{sgmf}(s)$ is applied to instead symbol function $\mathrm{sgn}(s)$. The expression of $\mathrm{sgmf}(s)$ is

$$\mathrm{sgmf}(s)=\begin{cases}2\left(\dfrac{1}{1+e^{-as}}-\dfrac{1}{2}\right) & |s|\le\varepsilon\\ \mathrm{sgn}(s) & |s|>\varepsilon\end{cases} \tag{59}$$

where ε is the boundary layer, and the constant $a>0$ is inversely proportional to ε. ε is assigned to 0.6 and $a=8/\varepsilon$.

For ease of differentiation, the guidance law proposed by Kumar is denoted as "NTSM", and the guidance law derived in this paper is called "ESODSC". After carefully adjusting the parameters, the simulation results under situation 3 are shown in Fig.15-19, and also tabulated in Table Ⅲ-Ⅳ.

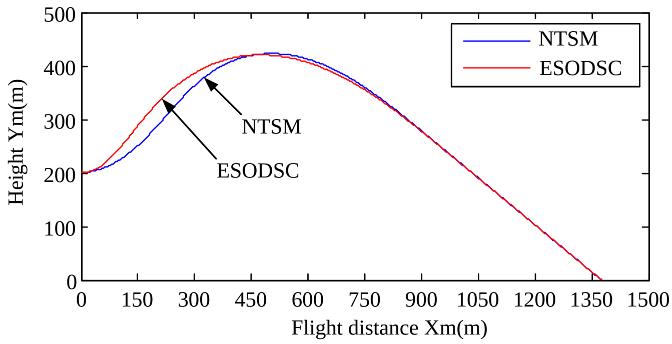

Fig.15. Curves of missile trajectories

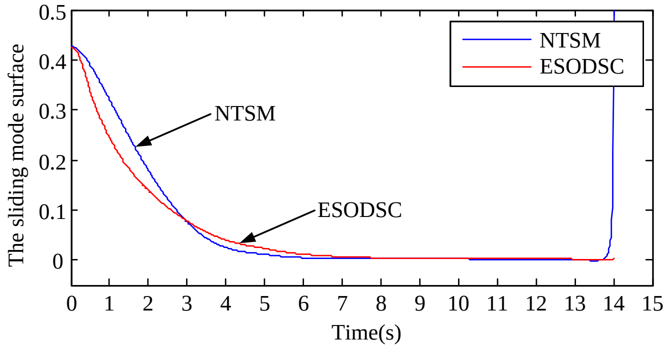

Fig.16. Curves of nonsingular terminal sliding mode surfaces

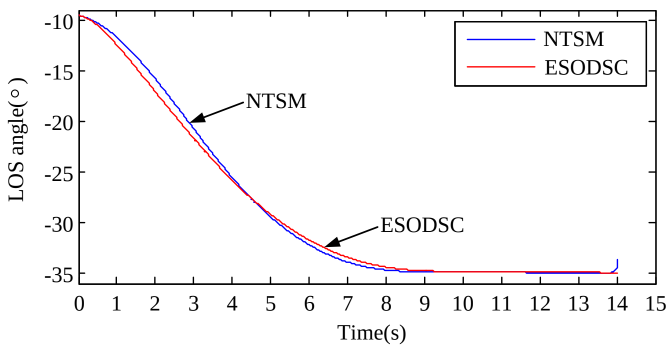

Fig.17. Curves of LOS angles

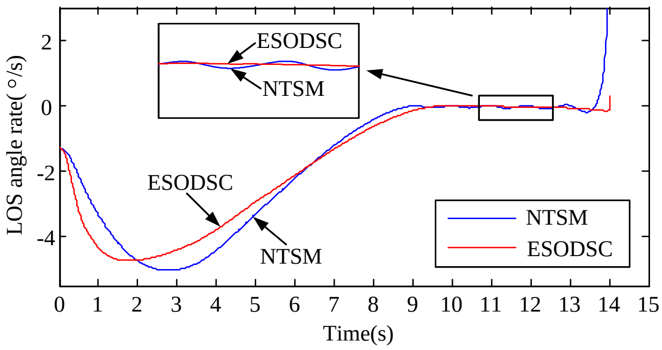

Fig.18. Curves of LOS angle rates

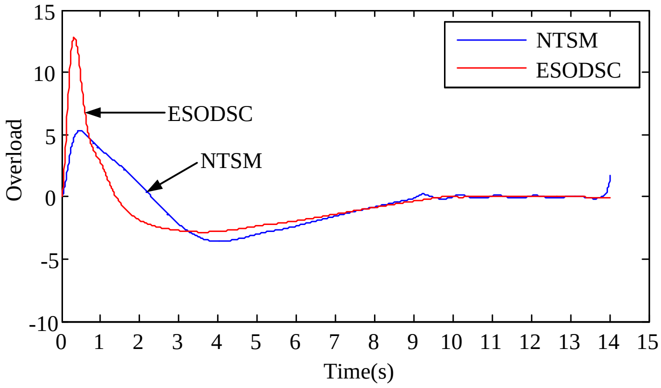

Fig.19. Curves of missile overloads

TABLE III
THE MOMENTS THAT DIFFERENT INDICATORS ENTER CONVERGENCE AREAS OF GUIDANCE LAWS

Guidance Law	The Moments That Indicators Below Firstly Enter Into The Convergence Ranges (s)			
	Sliding Mode $\|s\| < 0.02$	LOS Angle Rate (rad/s) $\|\dot{q}\| < 0.1$	LOS Angle(°) $\|q - q_d\| < 0.5$	Overload $\|N\| < 0.3$
NTSM	4.27	8.64	7.69	8.78
ESODSC	5.25	9.17	7.96	9.12

TABLE IV
$R(t_f)$ AND $q(t_f)$ UNDER THREE TARGET MOTION SITUATIONS

Guidance Law	$R(t_f)$ (m)	$q(t_f)$ (°)
NTSM	0.6103	-33.58
ESODSC	0.1066	-34.97

In order to compare performances of the two laws more directly, adjust parameters to make the missiles using the two laws have similar flight trajectories. In simulation, the landing times of missiles are both 14.03s. As can be observed in Fig.15-19, both guidance laws can enforce the LOS angles and LOS angle rates to approach zero in a finite time to satisfy the attack angle constraint. Similarly, the terminal overload requirements of these two guidance laws are both small and close to zero in the end. It can be easily observed that the convergence rates of sliding mode surface, LOS angle, LOS angle rate, and overload of ESODSC are all slower than those of NTSM. However, the convergence stability of ESODSC is better than NTSM, and the parameters variation of ESODSC is smaller than NTSM.

In the first half of simulation, drawing a comparison between ESODSC and NTSM, the convergence rates of sliding mode surface and missile-target LOS angle in ESODSC are faster. Besides, missile-target LOS angle rate and overload of ESODSC are larger. After a period of time, the convergence rates of the above indices of NTSM exceed the ESODSC. The reason for these phenomena is that the ESODSC is designed with a fast power reaching law. When the tracking error of system state is large, the exponential reaching term of ESODSC is dominant, then, the rapid increase of the control quantity not only improves the convergence rate, but also reduces the tracking error. At this time, the exponential reaching term of ESODSC is better than the constant reaching term of NTSM in terms of reaching speed. With the decrease of tracking error, the power reaching term of ESODSC takes the leading role, which leads to the diminution of control quantity and the slow convergence rate. In the mean while, the constant reaching term of NTSM is larger, which results in that the control quantity and convergence rate of NTSM exceed those of ESODSC. Along with the further decrease of tracking error, the system states converge to the sliding mode surface and approach near zero. Since the two kinds of guidance laws adopt the same non-singular terminal sliding mode surface in the form and parameter setting, the convergence performance is almost the same in the end.

However, the miss distance and terminal attacking angle are the two critical indices, which directly determine the attacking effect. As can be seen from Table III, the convergence times of sliding mode surface, LOS angle rate and LOS angle of NTSM are smaller than those of ESODSC. The reason for these phenomena is that the value of constant reaching term of NTSM is larger. However, because the NTSM does not consider the autopilot dynamic lag, the above indices will fluctuate after convergence, and divergence will occur before hitting the target, which may cause the large miss distance and angle error. In Table IV, the miss distances of NTSM and ESODSC are 0.6103m and 0.1066m, respectively, and the LOS angle errors of NTSM and ESODSC are -1.42 °and 0.03 °, respectively. The above analysis shows that compared with traditional nonsingular terminal sliding mode, the guidance law presented in this paper can get smaller miss distance and more precise preset attack angle, which has a better attack effect on the target.

VI. CONCLUSION

Considering autopilot dynamic lag, a guidance law with attack angle constraint is proposed by nonsingular terminal sliding mode control and dynamic surface control. The ESO with improved fal function is applied for estimating the derivatives of virtual control quantities and disturbance terms. According to Lyapunov stability theory, it is proved that all states in the closed-loop system converge into a little neighborhood near zero in finite time. Accordingly, simulation results indicate that the proposed guidance law is able to intercept stationary and maneuvering targets at desired attack angle within a finite time.

REFERENCES

[1] M. Kim, K. V. Grider, "Terminal guidance for impact attitude angle constrainted flight trajectories," *IEEE Transactions on Aerospace and Electronic Systems*, vol. 9, no.5, 1973, pp. 852-859.

[2] D. Liu and Z. K. Qi, "Impact angle and final position constrained optimal guidance law," *Journal of Beijing Institute of Technology*, vol. 21, no. 3, 2001, pp. 278-281.

[3] F. Gao, S. J. Tang, J. Shi, and J. Guo, "A bias proportional navigation guidance law based on terminal impact angle constraint," *Transactions of Beijing Institute of Technology*, vol. 34, no. 3, 2014, pp. 277-282.

[4] Y. A. Zhang, G. X. Ma, and A. L. Liu, "Guidance law with impact time and impact angle constraint," *Chinese Journal of Aeronautics*, vol. 26, no. 4, 2013, pp. 960-966.

[5] V. Shaferman and T. Shima, "Linear quadratic guidance laws for imposing terminal intercept angle," *Journal of Guidance, Control, and Dynamics*, vol. 31, no. 5, 2008, pp. 1400-1412.

[6] Y. S. Zhang, H. G. Ren, Z. Wu, and T. W. Wu, "On sliding mode variable structure guidance law with terminal angular constraint," *Electronics Optics &Control*, vol. 19, no. 1, 2012, pp. 66-68.

[7] J. X. Chi, H. Zhao, X. W. Weng, and Y. B. Xuan, "A terminal guidance law of the self-adaption variable structure considering angular constraint for air-to-ground attacking," *Fire Control & Command Control*, vol. 37, no. 4, 2012, pp. 34-36.

[8] Z. H. Man and X. H. Yu, "Terminal sliding mode control of MIMO linear systems," *IEEE Trans. On Circuits and Systems I: Fundamental Theory and Applications*, vol. 44, no. 11, 1997, pp. 1065-1070.

[9] Y. Q. Wu, X. H. Yu, and Z. H. Man, "Terminal sliding mode control design for uncertain dynamic systems," *Systems &Control Letters*, vol. 34, 1998, pp. 281-288.

[10] X. Y. Xu and H. Lin, "Control of single-axis roll stabilized servo platform based on adaptive nonsingular and fast terminal dynamic sliding mode," *Journal of Chinese Inertial Technology*, vol. 21, no. 6, 2013, pp. 726-731.

[11] H. B. Zhou, S. M. Ong, M. Y. Xu, and J. H. Song, "Design of terminal sliding mode guidance law with attack angle constraint," *25th Chinese Control and Decision Conference*, Piscataway, NJ: IEEE Press, 2013, pp. 556-560.

[12] S. R. Kumar, S. Rao, and D. Ghose, "Nonsingular terminal sliding mode guidance with impact angle constraints," *Journal of Guidance, Control and Dynamics*, vol. 37,no.4, 2014, pp. 1114-1130.

[13] D. Swaroop, J. K. Hedrick, P. P. Yip, and J. C. Gerdes, "Dynamic surface control for a class of nonlinear systems," *IEEE Transactions on Automatic Control*, vol.45, no. 10, 2000, pp. 1893-1899.

[14] Y. Zhang, J. Guo, S. J. Tang, W. Shang, and H. Q. Zhang, "A novel sliding mode guidance law with impact angle constraint for maneuvering target interception," *Acta Armamentar II*, vol. 36, no. 8, 2015, pp. 1443-1457.

[15] P. P. Qu and D. Zhou, "Guidance law incorporating second-order dynamics of missile autopilots," *Systems Engineering and Electronics*, vol. 33, no. 10, 2011, pp. 2263-2267.

[16] J. Yang, X. G. Wang, Z. Y. Wang, and S. J. Chang, "Robust terminal guidance law with autopilot lag and impact angle constraints," *Acta Armamentar II*, vol. 38, no. 5, 2017, pp. 900-909.

[17] H. J. Wang, J. L. Jian, H. M. Lei, X. Li, and W. D. Ma, "A new sliding mode guidance law based on extended state observer," *Journal of Solid Rocket Technology*, vol. 38, no. 5, 2015, pp. 622-627.

[18] S. F. Xiong, W. H. Wang, X. D. Liu, S. Wang, and L. Wu, "Impact angle guidance law considering missile's dynamics of autopilot," *Control and Decision*, vol. 30, no.4, 2015, pp. 586-592.

[19] S. Sun, H. M. Zhang, and D. Zhou, "Sliding mode guidance law with autopilot lag for terminal angle constrained trajectories," *Journal of Astronautics*, vol. 34, no. 1, 2013, pp. 69-78.

[20] Z. S. Diao and J. Y. Shan, "Continuous finite-time stabilization guidance law for terminal impact angle constrained flight trajectory," *Journal of Astronautics*, vol. 35, no. 10, 2014, pp. 1141-1149.

[21] D. Y. Chwa, J. Y. Choi, and S. G. Anavatti, "Observer-based adaptive guidance law considering target uncertainties and control loop dynamics," *IEEE Trans. On Control Systems Technology*, vol. 14, no. 1, 2006, pp. 112-123.

[22] K. M. Ma, "Non-smooth design and implementation of high-precision guidance laws," *Journal of Ballistics*, vol. 25, no.2, 2013, pp. 1-5.

[23] S. P. Bhat and D. S. Bernstein, "Finite-time stability of homogeneous systems," *Proceedings of American Control Conference*, Albuquerque, New Mexico, US: IEEE, 1997, pp. 2513-2514.

[24] S. Yu, X. Yu, B. Shirinzadeh, and Z. Man, "Continuous finite-time control for tobotic manipulators with terminal sliding mode," *Automatica*, vol. 41, no. 11, 2005, pp. 1957-1964.

[25] C. Qian and W. Lin, "Non-Lipschitz continuous stabilizers for nonlinear systems with uncontrollable unstable linearization," *Systems & Control Letters*, vol. 42, no. 3, 2001, pp. 185-200.

[26] J. Q. Han, "A class of extended state observers for uncertain systems," *Control and Decision*, vol. 10, no. 1, 1995, pp. 85-88.

[27] Y. Huang and J. Q. Han, "Analysis and design for the second order nonlinear continuous extended state observer," *Chinese Science Bulletin*, vol. 45, no. 21, 2000, pp. 1938-1944.

[28] J. Q. Han, "From PID to active disturbance rejection control," *IEEE Trans on Industrial Electronics*, vol. 56, no. 3, 2009, pp. 900-906.

[29] Y. Yao and Y. H. Wang, "Acceleration estimation of maneuvering targets based on extended state observer," *Systems Engineering and Electronics*, vol. 31, no. 11, 2009, pp. 2682-2692.

[30] B. Z. Guo and Z. L. Zhao, "On the convergence of an extended state observer for nonlinear systems with uncertainty," *System & Control Letters*, vol. 60, no.6, 2011, pp. 420-430.

[31] Y. Huang and J. Q. Han, "Analysis and design of nonlinear continuous second order state observer," *Chinese Science Bulletin*, vol. 45, no. 13, 2000, pp. 1373-1379.

[32] Y. H. Wang, Y. Yao, and K. M. Ma, "Error estimation of second order extended state observer," *Journal of Jilin University(Engineering and Technology Edition)*, vol. 40, no.1, 2010, pp. 143-147.

[33] X. Liu, X. X. Sun, and Z. Hao, "A new discrete-time form of optimal tracking differentiator," *Information and Control*, vol. 42, no. 6, 2013, pp. 729-734.